Hindawi Publishing Corporation
Journal of Nanomaterials
Volume 2016, Article ID 4103847, 5 pages
http://dx.doi.org/10.1155/2016/4103847

Research Article

Stepwise Growth of Hollow Hexagonal α-Fe_2O_3 Nanocrystals

Liqun Wang, Sen Yang, Yin Zhang, Jieqiong Wang, Minwei Xu, Xiaoping Song, and Xuegang Lu

School of Science, MOE Key Laboratory for Nonequilibrium Synthesis and Modulation of Condensed Matter, Xi'an Jiaotong University, Xi'an, Shaanxi 710049, China

Correspondence should be addressed to Yin Zhang; yzhang18@xjtu.edu.cn and Xuegang Lu; xglu@xjtu.edu.cn

Received 26 July 2016; Accepted 4 October 2016

Academic Editor: Fusheng Ma

Magnetic nanocrystals have attracted much attention in various fields because of their fundamental size and shape dependent magnetism and many technological applications. In this study, hollow hexagonal α-Fe_2O_3 nanocrystals were synthesized using a normal hydrothermal method. A full growth evolution map of nanocrystals with different shapes was investigated to elucidate the growth mechanism. We had demonstrated the growth mechanism using the selective adsorption and dissolution theory and interestingly found that K^+ cations were also a key point during the process of α-Fe_2O_3 nanocrystals growing. At last, the magnetic properties of the hexagonal α-Fe_2O_3 nanocrystals were also investigated.

1. Introduction

In the past decade, efforts have been made to control the growth of nanomaterials because different size and shape of nanocrystal can provide different properties that are suitable for various applications such as sensing, biotechnology, and energy conversion [1–3]. To improve performance for specific applications, a variety of methods have been attempted to control the microstructure of nanomaterials. For example, Zhang et al. used a simple wet chemistry to synthesize different ZnO crystals, including disk-like, flower-like, and nanorod flower-like structure, and investigated the parameters' impact during the crystal growth [4]. Besides normal oxides, some other novel heterostructures such as dumbbell-like α-Fe_2O_3/Ag/AgX (X = Cl, Br, and I) could also be obtained via an *in situ* oxidation reaction and self-assembly process [5]. Thus, it is fundamentally significant to realize the mechanism and method to grow nanomaterials. In our previous study, hollow cage-like α-Fe_2O_3 were successfully synthesized by an electrospinning technique and they exhibited a ferromagnetic behavior and possess high saturation magnetization [6]. Among them, controlled crystallization is regarded as an effective synthetic strategy because of its potential to produce well-defined particles with unique and controlled structures [7]. As the process of nucleation and growth of nanocrystals is highly sensitive to external environment, it can be easily influenced by adjusting the experimental parameters. In such process, the orientation of crystal growth is mainly driven by the surface energy, and the final product always has the minimum surface energy in a certain environment [8, 9]. Therefore, to form specific crystals, impurities or additives are usually added to efficiently tailor the structure and morphology because these ions or atoms will interact with crystals faces during the growth at a certain atomic configuration and affect their stability in terms of surface energy.

Hematite (α-Fe_2O_3), the most stable iron oxide, has tremendous scientific and technological importance because of its use in catalysts, magnetic materials, gas sensors, and lithium-ion batteries [10, 11]. The magnetism of α-Fe_2O_3 exhibits a first-order magnetic transition at Morin temperature (T_M) besides the common Néel transition of antiferromagnetic materials [12]. Similar to other nanomaterials, the decrease in particle size significantly affects the magnetic behavior of α-Fe_2O_3. Moreover, different structures of α-Fe_2O_3, such as nanorods, nanowires, and nanotubes, also have an impact on magnetic properties [11, 13]. Herein, we report a solution-based method involving a multi-ions assisted hydrothermal route to produce α-Fe_2O_3 nanocrystals with structure evolution from nanorod to hexagonal nut

and hollow hexagonal nut and back to hexagons again. The growth mechanism of the hollow hexagonal α-Fe_2O_3 was investigated and it was found that K^+ cations played an important role in this process. Moreover, an unusual *M-T* curve was observed for the nanocrystals.

2. Materials and Methods

First, different concentrations of $FeCl_3 \cdot 6H_2O$ (0.43 mM), $KH_2PO_4 \cdot H_2O$ (0.01 mM), and Na_2SO_4 (0.01 mM) solutions were prepared. Then, specific amounts of aqueous solutions (20 mL $FeCl_3 \cdot 6H_2O$, 12 mL $KH_2PO_4 \cdot H_2O$, and 48 mL Na_2SO_4, resp.) were mixed and vigorously stirred until a homogeneous solution was obtained. The resulting mixture was transferred to a 100 mL Teflon-lined stainless steel autoclave and heated at 220°C for a specified time (1, 4, 12, and 24 hours) to elucidate the growth mechanism. Brick-red precipitates were obtained by centrifugation and washed thoroughly with deionized water and ethanol for several times.

The crystal structure of the as-synthesized samples was determined by powder X-ray diffraction (XRD) on a Bruker D8 Advance X diffractometer using Cu Kα radiation. Morphology was analyzed by field emission scanning electron microscopy (FESEM, JSM-7000F). High-resolution images and selected-area electron diffraction (SAED) patterns were performed with a high-resolution transmission electron microscopy (HRTEM, JEOL-2100) operating at 200 kV. Magnetization data was taken using a Quantum Design SQUID magnetometer. The temperature dependence of magnetization (*M-T*) was measured under zero-field-cooling (ZFC) and field-cooling (FC) conditions from 2 K to 300 K by applying a magnetic field of 100 Oe. The field dependence of magnetization (*M-H*) was examined at 2 and 300 K with continuous field sweeping from −30 to 30 kOe.

3. Results and Discussions

Figure 1 shows the XRD spectrum of the hollow hexagonal α-Fe_2O_3 nanocrystals. All the peaks can be indexed to the hexagonal phase of α-Fe_2O_3 (the standard PDF positions of α-Fe_2O_3 were shown in Figure 1 using the black vertical line) with lattice constants of a = 5.00 Å and c = 13.62 Å. No peak from impurities or inorganic ions was observed, indicating that the powder was well crystallized. The morphologies of the samples with different reaction times were observed by SEM to elucidate the formation mechanism.

From the SEM images (Figure 2), we can know that the α-Fe_2O_3 nanocrystals formed capsule-like nanorods with depression in the center at the first hour; after 4 h, the crystals clearly dissolved along the axis of the hexagonal particles, and the central depression became a hole gradually; 12 hours later, the products of hexagonal crystals with a central hole were observed. Moreover, the size and shape of the hexagonal crystals were further well defined at this time. The final nanonuts had a larger diameter and smoother surface than the capsule-shaped precursors, and the central hole grew larger too, indicating that the recrystallization also accompanied the "dissolution" of the surface. Interestingly,

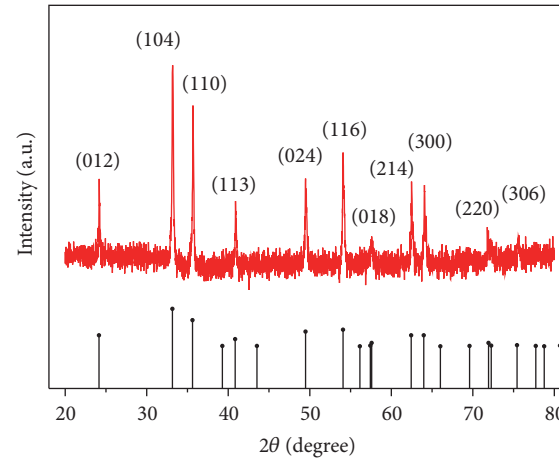

Figure 1: X-ray diffraction spectrum of hexagonal α-Fe_2O_3 nanocrystals.

when the reaction lasted for 24 h, the central holes of the nanonuts were filled up again and the structure at this time was very similar to that of 12 h.

The low-magnification TEM images (Figure 3(a)) clearly show a perfectly hexagonal structure with a similarly shaped hole inside, and the diameter of the hexagonal nanonuts was approximately 100 ± 2 nm. Interestingly, the hollow hole also shows a hexagonal structure as outside, although that hexagon is not observed very clearly. The outer and inner edges marked by dot-circles in Figure 3(a) were further investigated by HRTEM. These nanonut crystals have an interplanar distance of 0.251 nm, consistent with d_{110} spacing of a pure hexagonal hematite. The SAED pattern shown in the inset of Figure 3(b) confirms that the outer and inner hexagons both have a rhombohedral α-Fe_2O_3 structure. This also indicates that same adsorption and dissolution reaction orientation are conducted during the hydrothermal process.

Herein, the growth mechanism is contributing to the selective adsorption and dissolution of ionic ligands on different crystal planes. It is known that phosphate and sulfate ions adsorb on (110) and (100) surface of α-Fe_2O_3, mainly by forming binuclear, bidentate complexes with two singly coordinated hydroxyl groups, even though other types of surface complexes are possible [14, 15]. Jia et al. utilized the cooperative action of phosphate and sulfate ions to synthesize single α-Fe_2O_3 crystals previously. The products had a ring-like structure with a circular shape and central hole [11]. In this case, we found that addition of K^+ ions into the reaction environment can also affect crystal growth orientation and the final morphology of α-Fe_2O_3.

In the first stage, the presence of phosphate ions helps in the growth of capsule-like nanorod structure, where [001] direction is preferred and (110) and (100) prism planes are maintained. Here, the temperature of the solution was not sufficiently high for the redox reaction. Simultaneously, the phosphate anions hindered the coordination reaction with the exposed Fe^{3+} ions on the initial α-Fe_2O_3 nuclei. Therefore, sulfate ions slightly affected the growth of α-Fe_2O_3 nanocrystals. Then, in an acidic environment and at

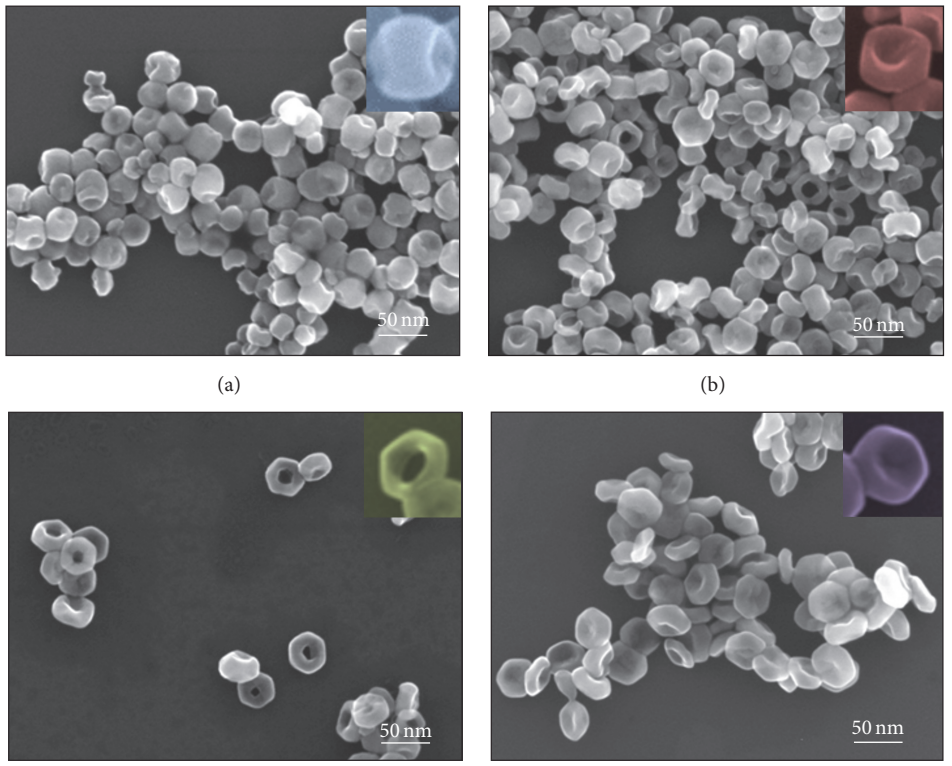

Figure 2: Morphological evolution of hollow hexagonal α-Fe_2O_3 nanocrystals with different reaction times, as revealed by the SEM images of the products prepared at 220°C for (a) 1, (b) 4, (c) 12, and (d) 24 h. Insets give the selected magnification of product at each reaction time.

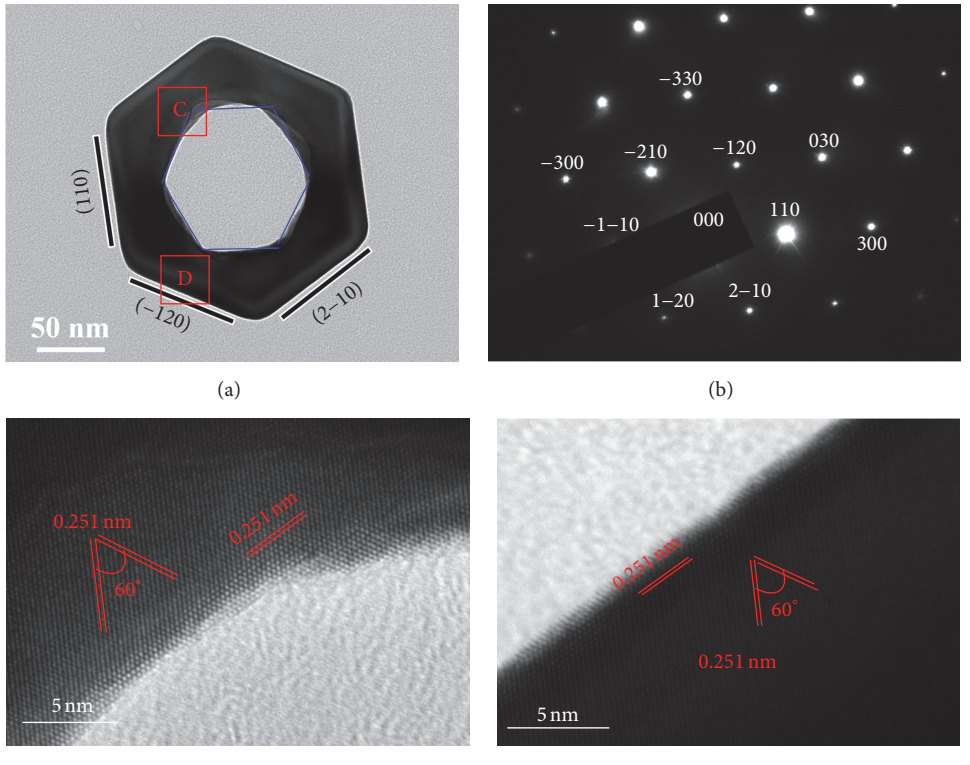

Figure 3: TEM image of single hexagonal α-Fe_2O_3 nanostructure; (b) SAED pattern of α-Fe_2O_3 particle in (a); the HRTEM images of the selected areas in (a) are shown in (c) and (d).

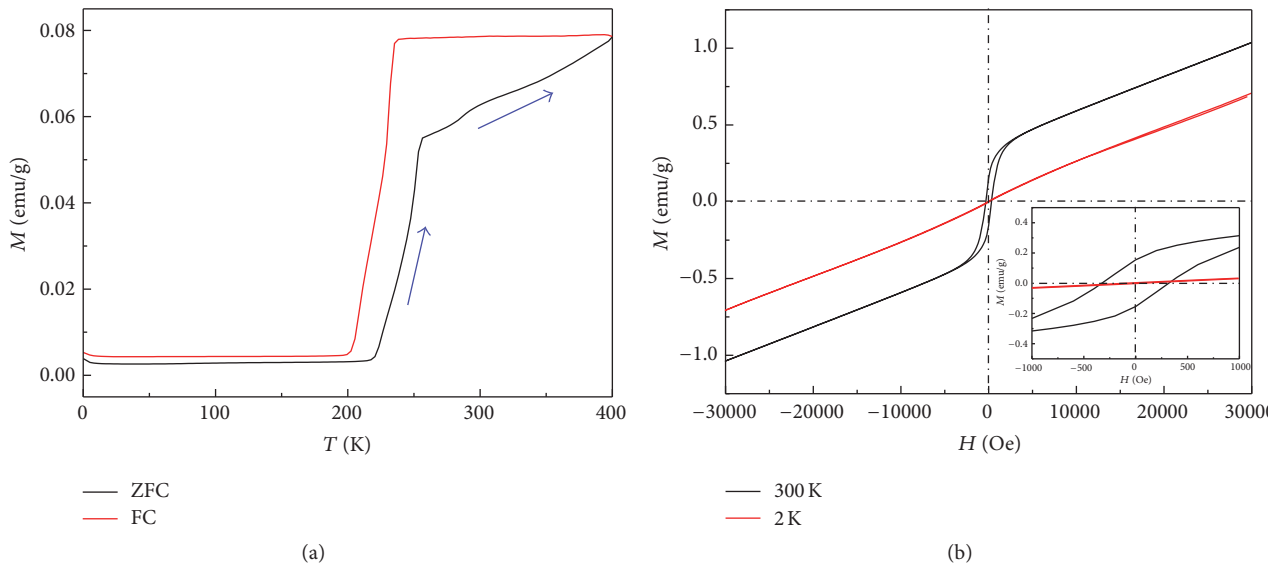

FIGURE 4: (a) Temperature and field dependence of the magnetization. (b) Magnetic hysteresis loops at 300 K and 2 K. The inset in (b) is the expanded view of the loop.

a high temperature, the tips of the capsule-shaped nanorods started to dissolve along the [001] direction, as the (001) plane was almost entirely exposed to the solution [14–16]. In this stage, the sulfate ions acted as a shape controller to induce the anisotropic growth. With the crystal growth, the concentration of Fe^{3+} ions in the solution gradually decreased to a very low level, and the exposed Fe^{3+} ions on the formed nanorods began to react with the sulfate ions; that is, in the dissolution step, the redox reaction is still dominated by the sulfate coordination effect with the detached ferric ions. Thus, the formation of the initial hexagonal-nanorods particles can be explained; however, the change of the shape from nanorods to hollow hexagons instead of nanorings cannot be followed by such mechanism.

It is always believed that additives cations do not participate in adsorption and dissolution processes [14]. In comparison to the previous report, however, we only introduced some K^+ ions into the solution. During the formation of hollow hexagonal nanocrystals, K^+ ions affected the dissolution of sulfate ions at both outer and inner edges. This process would ultimately make a hole in the particle as long as the reaction time is adequate. The HRTEM analysis shows that the inner and outer wall surfaces are composed of the same planes; therefore, the wall surfaces are effectively protected by the adsorption of phosphate and sulfate ions. Finally, single hollow hexagonal α-Fe_2O_3 nanocrystals with a hexagonal inner hole were formed. Notably, for longer reaction times, the adsorption and desorption of phosphate or sulfate ions on the surface of α-Fe_2O_3 crystals reach the equilibrium, and the dissolution and recrystallization processes also gradually reach the equilibrium. Thus, α-Fe_2O_3 crystals become hexagons back and the hole disappears.

Figure 4 shows the temperature and field dependence of the zero-field-cooling (ZFC) and field-cooling (FC) magnetic susceptibilities of the α-Fe_2O_3 nanocrystals under an applied field of 100 Oe. Normally, bulk hematite α-Fe_2O_3 undergoes a transition from the low-temperature antiferromagnetic phase to a weakly ferromagnetic phase at 263 K, namely, Morin transition. Herein, the hexagonal nanostructures have a Morin transition at 203 K, lower than that of bulk and other nanostructures [10]. This result is consistent with the expected trend of decreasing T_M with the decrease in particle size. At the same time, we had observed large thermal hysteresis in T_M (~16 K) between the cooling and heating measurements, indicating that Morin transition is a first-order transition. During the warming, two slight different slopes were unexpectedly observed in the ZFC curve at Morin transition (blue line in Figure 4(a)). This is probably attributed to the different domains behaviors in the outer and inner edges of hexagons. In Figure 4(b), two magnetic hysteresis loops at room temperature (300 K) and low temperature (2 K) are compared. For the present nanocrystals, the obvious hysteresis at 300 K suggests that the sample is in a weak ferromagnetic state with a coercive field of approximately 450 Oe and remnant magnetization of 1.9×10^{-2} $emug^{-1}$, whereas from the magnetic hysteresis loops at 2 K, the nanocrystals are antiferromagnetic with zero saturation magnetization. The whole result is also consistent with the FC-ZFC curves.

4. Conclusion

In summary, this paper presents a simple hydrothermal approach to fabricate crystalline hollow hexagonal α-Fe_2O_3 nanocrystals in high yield. To obtain the final hollow product, the nanocrystal undergoes a shape evolution from capsule-like cylinder and hexagonal nut with center depressed center to hollow hexagonal nanocrystal finally. We demonstrate that K^+ ions have played an important role in controller of shape. The magnetic property investigation shows that

the as-prepared hollow α-Fe_2O_3 nanostructures exhibit a ferromagnetic behavior and decreased Morin temperature.

Competing Interests

The authors declare that there are no competing interests regarding the publication of this paper.

Acknowledgments

The authors are grateful for financial support from the National Natural Science Foundation of China (nos. 51172178, 51222104, 51371134, and 51501142), the project of Innovative Team of Shaanxi Province (no. 2013KCT-05), and China Postdoctoral Science Foundation (Grant no. 2015M580838).

References

[1] A. S. Aricò, P. Bruce, B. Scrosati, J.-M. Tarascon, and W. Van Schalkwijk, "Nanostructured materials for advanced energy conversion and storage devices," *Nature Materials*, vol. 4, no. 5, pp. 366–377, 2005.

[2] X. Chen and S. S. Mao, "Titanium dioxide nanomaterials: synthesis, properties, modifications and applications," *Chemical Reviews*, vol. 107, no. 7, pp. 2891–2959, 2007.

[3] V. L. Colvin, "The potential environmental impact of engineered nanomaterials," *Nature Biotechnology*, vol. 21, no. 10, pp. 1166–1170, 2003.

[4] H. Zhang, D. Yang, S. Z. Li et al., "Controllable growth of ZnO nanostructures by citric acid assisted hydrothermal process," *Materials Letters*, vol. 59, no. 13, pp. 1696–1700, 2005.

[5] L. Sun, W. Wu, Q. Tian et al., "*In situ* oxidation and self-assembly synthesis of dumbbell-like α-Fe_2O_3/Ag/AgX (X = Cl, Br, I) heterostructures with enhanced photocatalytic properties," *ACS Sustainable Chemistry & Engineering*, vol. 4, no. 3, pp. 1521–1530, 2016.

[6] L. Wang, X. Lu, C. Han, R. Lu, S. Yang, and X. P. Song, "Electrospun hollow cage-like α-Fe_2O_3 microspheres: synthesis, formation mechanism, and morphology-preserved conversion to Fe nanostructures," *CrystEngComm*, vol. 16, no. 46, pp. 10618–10623, 2014.

[7] S. Kumar and T. Nann, "Shape control of II–VI semiconductor nanomaterials," *Small*, vol. 2, no. 3, pp. 316–329, 2006.

[8] N. Jana, G. Latha, and J. M. Catherine, "Seed-mediated growth approach for shape-controlled synthesis of spheroidal and rod-like gold nanoparticles using a surfactant template," *Advanced Materials*, vol. 13, no. 18, pp. 1389–1393, 2001.

[9] M. Grzelczak, J. Pérez-Juste, P. Mulvaney, and L. M. Liz-Marzán, "Shape control in gold nanoparticle synthesis," *Chemical Society Reviews*, vol. 37, no. 9, pp. 1783–1791, 2008.

[10] J. Chen, L. N. Xu, W. Y. Li, and X. L. Gou, "α-Fe_2O_3 nanotubes in gas sensor and lithium-ion battery applications," *Advanced Materials*, vol. 17, no. 5, pp. 582–586, 2005.

[11] C.-J. Jia, L.-D. Sun, F. Luo et al., "Large-scale synthesis of single-crystalline iron oxide magnetic nanorings," *Journal of the American Chemical Society*, vol. 130, no. 50, pp. 16968–16977, 2008.

[12] F. Bødker, M. F. Hansen, C. B. Koch, K. Lefmann, and S. Mørup, "Magnetic properties of hematite nanoparticles," *Physical Review B*, vol. 61, no. 10, pp. 6826–6838, 2000.

[13] C. Z. Wu, P. Yin, X. Zhu, C. Z. OuYang, and Y. Xie, "Synthesis of hematite (α-Fe_2O_3) nanorods: diameter-size and shape effects on their applications in magnetism, lithium ion battery, and gas sensors," *The Journal of Physical Chemistry B*, vol. 110, no. 36, pp. 17806–17812, 2006.

[14] W. Wu, X. H. Xiao, S. F. Zhang et al., "Large-scale and controlled synthesis of iron oxide magnetic short nanotubes: shape evolution, growth mechanism, and magnetic properties," *Journal of Physical Chemistry C*, vol. 114, no. 39, pp. 16092–16103, 2010.

[15] J. Liu, Z. Wu, Q. Tian, W. Wu, and X. Xiao, "Shape-controlled iron oxide nanocrystals: synthesis, magnetic properties and energy conversion applications," *CrystEngComm*, vol. 18, no. 34, pp. 6303–6326, 2016.

[16] B. L. Lv, Y. Xu, D. Wu, and Y. H. Sun, "Single-crystal α-Fe_2O_3 hexagonal nanorings: stepwise influence of different anionic ligands (F-and SCN-anions)," *Chemical Communications*, vol. 47, no. 3, pp. 967–969, 2011.